ARTICLE

Assay Related Target Similarity (ARTS) - Chemogenomics Approach for Quantitative Comparison of Biological Targets
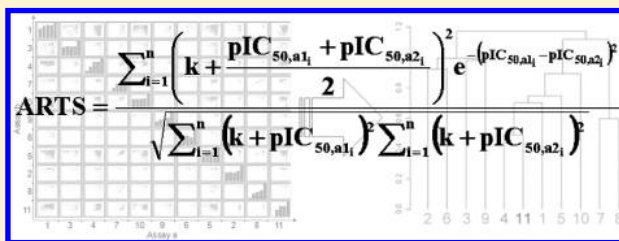
Michael Bieler,*,† Ralf Heilker,† Herbert Köppen,† and Gisbert Schneider‡

†Lead Identification and Optimization Support, Boehringer Ingelheim Pharma GmbH & Co. KG, Birkendorfer Strasse 65, D-88397 Biberach, Germany

‡Swiss Federal Institute of Technology (ETH), Institute of Pharmaceutical Sciences, Wolfgang-Pauli-Strasse 10, 8093 Zürich, Switzerland

Ⓢ *Supporting Information*

ABSTRACT: Computer-based chemogenomics approaches compare macromolecular drug targets based on their amino acid sequences or derived properties, by similarity of their ligands, or according to ligand-target interaction models. Here we present ARTS (*Assay Related Target Similarity*) as a quantitative index that estimates target similarity directly from measured affinities of a set of probe compounds. This approach reduces the risk of deducing artificial target relationships from mutually inactive compounds. ARTS implements a scoring scheme that matches intertarget similarity based on dose–response measurements. While all experimentally derived target similarities have a tendency to be data set-dependent, we demonstrate that ARTS depends less on the used data set than the commonly used Pearson correlation or Tanimoto index.

$$\text{ARTS} = \frac{\sum_{i=1}^{n} \left(k + \frac{pIC_{50,a1_i} + pIC_{50,a2_i}}{2} \right)^2 e^{-\left(pIC_{50,a1_i} - pIC_{50,a2_i} \right)^2}}{\sqrt{\sum_{i=1}^{n} \left(k + pIC_{50,a1_i} \right)^2 \sum_{i=1}^{n} \left(k + pIC_{50,a2_i} \right)^2}}$$

■ INTRODUCTION

Historically, two different concepts have been followed to describe target similarity, based on the structures of i) drug targets[1,2] or ii) the properties of the ligands.[3−7] A third, more recently pursued model, is grounded on target-ligand interactions.[8−10] In 2000, Vertex Pharmaceuticals published a press release wherein they described an approach to '*rapidly and simultaneously design multiple lead classes of drugs directed at protein targets in gene families*', termed "chemogenomics", which has become a well-established concept ever since,[11,12] especially in the field of the G-protein coupled receptor (GPCR) families.[13,14] The term chemogenomics describes a procedure of linking information about several biological targets and small molecular weight effectors.[15] The idea behind this bridging of chemical and biological space is that closely related compounds should have similar biological profiles, and closely related targets should share similar compounds — or in other words: similar receptors bind similar ligands.[16] The crucial question is how to define "similarity" on the molecular level. It is not necessarily the similarity of the molecular graph, but the similarity of those features of the compounds that are responsible for the respective ligand–target interactions. And, as a consequence, the description of ligand similarity is inherently context-dependent and may differ from target to target. However, the description of target similarity in the context of ligand binding does not necessarily depend on sequence information only. The principle of chemogenomics can be applied in different ways:

(1) Binding sites, which are phylogenetically related should accommodate similar ligands, and known ligands for a certain target are valid starting points for identifying ligands that bind to closely related target macromolecules.[1,2]

(2) Compounds that bind to a certain target should possess common features that actually correspond to the binding site of the target. Binding sites of targets that are phylogenetically different but nevertheless share the same features should also be able to accommodate these compounds. This concept could enable drug repurposing or prediction of potential side effects.[17,18] Other applications compare and classify receptors based on binding sites by using sequence motifs or (putative) three-dimensional (3D) information, mostly focusing on those amino acids that are known to be essential for ligand recognition from site-directed mutagenesis studies. One of the first studies using sequence motifs was performed by Crossley et al., whose "thematic analysis" comprises groups of amino acids that are likely to be involved in ligand binding, on the basis of experimental data.[19,20]

(3) The activity of compounds at sets of targets (rather than a single individual target) can be used as an experimentally derived descriptor of the compound. *In vitro* fingerprints were first introduced by Kauvar et al.[21] and shortly afterward followed by *in silico* counterparts.[22] Such a descriptor can be used for similarity searching: Two compounds that are similar with respect to this representation (i.e., activities at *N* targets) should exhibit similar activity at

any additional target, even if the chemical structures of the compounds differ. Such a descriptor is independent from the chemical structure of the compounds and refers directly to their assay-relevant features. This concept can be helpful for the identification of new hits and lead candidates with similar activity profiles.

For somatostatin receptor subtype 5 (SST5R), Guba et al. retrieved an antagonist *via* a chemogenomics strategy based on affinity fingerprint similarity.[23,24] Attempts have been made to predict binding affinities of ligands for new targets based on known ligands of these targets, using methods of virtual screening. Poroikov et al.[25,26] and later Bender et al.[4,6] used a Bayesian approach to predict activity spectra and biological fingerprints, while Bock and Gough[27] and later Jacob and Vert[8] employed support vector machines. Mestres and co-workers have constructed a hypothetical ligand—receptor interaction network based on ligands against 25 nuclear receptors from literature and used it to predict previously unobserved ligand—receptor pairs.[28] Recently, Schneider and co-workers employed self-organizing fingerprints for the same task.[29] A comprehensive review on chemogenomics approaches is given elsewhere.[3]

From a chemogenomics perspective, similarity between different macromolecular targets is estimated from ligand binding affinities, which are encoded in an N-dimensional vector, where each element represents some kind of "activity flag" for one particular target. Often, these affinity vectors (fingerprints) are sparse with many inactive elements, and correlation-based similarity estimation tends to be biased by mutually inactive compounds.[30] As a consequence, there is a risk of deducing artificial target similarities. To overcome this problem we suggest a quantitative affinity-based similarity index that enables target similarity analysis taking the influence and peculiarities of the particular assays used for ligand activity determination into account: *Assay Related Target Similarity* (ARTS) is based on the hypothesis that two assays probing two different targets are similar if the binding of compounds occurs with a similar affinity. Here, we will show that ARTS is suited as a scoring scheme for interassay similarity. Only in those cases where the assay readout is primarily influenced by the interaction of the probe compound and the target, ARTS may even be considered as a measure for intertarget similarity. Furthermore we will demonstrate that ARTS-based hierarchical clustering of targets is less data set dependent than clustering based on correlation-based similarity scoring.

■ DATA AND METHODS

Data Set. The data matrix was composed of 3519 compounds, which were tested in dose response for binding to 11 diverse GPCR. For each GPCR target we selected approximately 110 known active compounds with different chemotypes from the Boehringer Ingelheim proprietary screening compound pool. Additional 210 analogs were selected as similar structures, based on Daylight[31] fingerprints (Tanimoto index > 0.7), to increase the number of compounds per chemotype.

SPA Assays. Scintillation Proximity Assay. (SPA) technology[32] is a frequently employed assay for high-throughput detection of ligand-GPCR complex formation. SPA employs microspheres that are doped with β-emission sensitive scintillants. These so-called 'scintillation beads' may be coated with bioreagents such as wheat germ agglutinin (WGA). WGA is

a lectin that binds to carbohydrate groups of glycolipids and glycoproteins in plasma membranes. Thus, membrane fragments from cells overexpressing a specific target GPCR may be immobilized on the surface of WGA-coated scintillation beads. In this way, the GPCRs are maintained in a lipid biomembrane that resembles their physiological environment. If a radioligand binds to the target GPCR on the scintillation bead, the scintillant on the bead surface emits light. If radioligand binding is inhibited by a test compound, the radio-emission of the unbound ligand will be absorbed by the surrounding aqueous solution and no light emission from the scintillation bead is induced. Unlike radioactive filtration assays or radio-immune assays, the unbound radioligand does not have to be removed prior to the scintillation measurement thereby enabling displacement assays under equilibrium conditions. As an alternative to the classical SPA beads, which are doped with a blue-light emitting scintillant, scintillation imaging beads have been designed that emit light in the red region.[33] These imaging beads enable the use of low temperature charge-coupled devices (CCDs) to measure scintillation from all wells of a microtiter plate (MTP) in parallel.[34,35] Due to the decreased measurement time, the scintillation imaging beads are generally preferred over conventional SPA beads in a high throughput drug discovery environment. In this work, both bead types have alternatively been employed, depending on the respective signal windows and signal-to-noise ratios during comparative assay development.

Eleven GPCR ligand binding assays were implemented in the SPA format. The 3519 panel test compounds were supplied by the Compound Logistics Group (Boehringer Ingelheim Pharma GmbH & Co. KG) at concentrations of 5 mg/mL in 100% dimethyl sulfoxide (DMSO). Test compounds were diluted in 100% DMSO to yield concentrations of 500 μg/mL, 158 μg/mL, 50 μg/mL, 15.8 μg/mL, and 1.58 μg/mL ('DMSO stock solutions'). Each stock solution was diluted 100-fold into the individual aqueous assay buffer of the respective GPCR assay format, producing test compound concentrations of 5 μg/mL, 1.58 μg/mL, 0.5 μg/mL, 0.158 μg/mL, 0.0158 μg/mL, and a residual 1% of DMSO in the final assay mixtures of radioligand, membrane fragments, and SPA beads. Membrane fragments from Chinese Hamster Ovary (CHO) cells overexpressing the respective GPCR of interest and the radioligands (Table 1) were purchased from PerkinElmer Life and Analytical Sciences (Waltham, MA, 02451, USA). All SPA beads were purchased from GE Healthcare UK Ltd. (Amersham Place, Little Chalfont, England). Measurements of classical SPA bead signals were carried out in a TopCount Microplate Scintillation Counter (PerkinElmer Life and Analytical Sciences, Waltham, MA, 02451, USA). Measurements of the imaging SPA beads were conducted with a LEADseeker Multimodality Imaging System (GE Healthcare UK Ltd.).

Pearson Correlation Coefficient. The Pearson correlation coefficient (eq 1) indicates the strength of a linear relationship between two variables. For a series of dose response measurements of n compounds at assay $a1$ and assay $a2$, written as $a1_i$ and $a2_i$, where $i = 1, 2, ..., n$, the Pearson correlation coefficient $r_{a1,a2}$ estimates the linear correlation of $a1$ with $a2$

$$r_{a1,a2} = \frac{\sum_{i=1}^{n} (pIC_{50,a1_i} - \overline{pIC_{50,a1}})(pIC_{50,a2_i} - \overline{pIC_{50,a2}})}{(n-1)S_{a1}S_{a2}}$$

(1)

Table 1. GPCRs, Radioligands, and Clusters for All Targets in This Analysis[a]

target number	GPCR	SwissProt entry name	cluster	radioligand
1	5-HT2C(e)	5HT2C_HUMAN	amines cluster	[N6-methyl-3H]-mesulergine
2	adenosine A1	AA1R_HUMAN	adenosine receptor cluster	[3H]-8-cyclopentyl-1,3-dipropylxanthine
3	adrenergic ss2	ADRB2_HUMAN	amines cluster	[125I]-(-) iodocyanopindolol
4	CB2	CNR2_HUMAN	lipids receptor cluster	CP-55,940, [side chain-2,3,4(N)-3H]-
5	CCR3	CCR3_HUMAN	chemokines receptor cluster	[125I]- recombinant human eotaxin
6	CRTH2	GPR44_HUMAN	chemoattractants receptor cluster	prostaglandin D2, [5,6,8,9,12,14,15—3H(N)]-
7	CXCR2	CXCR2_HUMAN	chemokines receptor cluster	[125I]-interleukin-8 (72 amino acids)
8	CXCR3	CXCR3_HUMAN	chemokines receptor cluster	([125I]-Tyr)-recombinant human I-TAC
9	muscarinic M3	ACM3_HUMAN	amines cluster	scopolamine methyl chloride, [N-methyl-3H]-
10	MCHR1	MCHR1_HUMAN	brain-gut peptides receptor cluster	([125I]-Tyr13)-melanin concentrating hormone (human, mouse, rat)
11	somatostatin sst4	SSR4_HUMAN	opiates receptor cluster	([125I]-Tyr11)-somatostatin 14

[a] Cluster names refer to the categories suggested by Surgand et al.[2]

where $\overline{pIC_{50,a1}}$ and $\overline{pIC_{50,a2}}$ are the sample means of the dose response values (pIC_{50}) of all compounds in $a1$ and $a2$. S_{a1} and S_{a2} are the sample standard deviations of the dose response values (pIC_{50}) of all compounds in $a1$ and $a2$. We calculated the Pearson correlation coefficient using the Pipeline Pilot[36] implementation of the statistics package R.[37]

Tanimoto coefficient. Given a series of dose response measurements of n compounds in assay $a1$ and assay $a2$, the Tanimoto coefficient is computed as given in eq 2

$$T_{a1,a2} = \frac{\sum_{i=1}^{n} pIC_{50,a1_i} pIC_{50,a2_i}}{\sum_{i=1}^{n} pIC_{50,a1_i}^2 + \sum_{i=1}^{n} pIC_{50,a2_i}^2 - \sum_{i=1}^{n} pIC_{50,a1_i} pIC_{50,a2_i}} \quad (2)$$

where $i = 1, 2, ..., n$ and $pIC_{50,a1_i}$ and $pIC_{50,a2_i}$ are the dose response values of compound i in the assay $a1$ and $a2$, respectively.

ARTS. We define two binding assays as *identical* if binding of the same compounds occurs with *identical* affinities, and two assays are *similar* if binding of the same compounds occurs with *similar* affinities. Further, we define that two assays that share potent ligands are more similar than two assays that share moderately or weakly binding ligands. With these assumptions we introduce a similarity score as the sum of all compounds i with $i = 1, 2, ..., n$, that are active at two targets (eq 3), weighted by an affinity-dependent score (eq 4)

$$Sim_{a1,a2} = \sum_{i=1}^{n} Score_{i,a1,a2} \quad (3)$$

where $Sim_{a1,a2}$ is the similarity of two assays $a1$ and $a2$, and $Score_{i,a1,a2}$ is the dose response dependent score of compound i for assays $a1$ and $a2$ (eq 4)

$$Score_{i,a1,a2} = \left(k + \frac{pIC_{50,a1_i} + pIC_{50,a2_i}}{2}\right)^2 e^{-(pIC_{50,a1_i} - pIC_{50,a2_i})^2} \quad (4)$$

where k is constant ($k = -4$), and $IC_{50,a1_i}$ and $IC_{50,a2_i}$ are the dose response values of compound i in assay $a1$ and $a2$, respectively.

As this raw similarity index (eq 3) is not normalized, we suggest a standardization factor by dividing the raw similarity

index by the square root of the self-similarities of both involved assays (eq 5)

$$Sim_{a1,a2_{Norm}} = \frac{Sim_{a1,a2}}{\sqrt{Sim_{a1,a1} Sim_{a2,a2}}} \quad (5)$$

where $Sim_{a1,a2_{Norm}}$ is the normalized similarity of assays $a1$ and $a2$. Because of some simplifications in eq 4 the self-similarity $Sim_{ax,ax}$ of an assay ax is rewritten (eq 6)

$$Sim_{ax,ax} = \sum_{i=1}^{n} (k + pIC_{50,ax_i})^2 \quad (6)$$

where pIC_{50,ax_i} is the dose response value of compound i in assay ax, and k is constant ($k = -4$).

Adjusted RAND-Index. In order to compare the results of two clustering procedures, a measure of agreement is needed. Since we compared a subset-based clustering with the clustering of the entire data set, measures of agreement between two partitions can be used.[38,39] Milligan and Cooper[40] evaluated different indices for the measurement of the agreement between two partitions in cluster analysis with different numbers of clusters and recommended the adjusted Rand index as the index of choice. Given a set of n objects $S = \{O_1,...,O_n\}$, suppose $U = \{u_1,...,u_R\}$ and $V = \{v_1,...,v_C\}$ represent two different partitions of the objects in S such that $\cup_{i=1}^{R} u_i = S = \cup_{j=1}^{C} v_j$ and $u_i \cap u_{i'} = \varnothing = v_i \cap v_{i'}$ for $1 \leq i \neq i' \leq R$ and $1 \leq j \neq j' \leq C$. Suppose that U is the partition based on clustering of the entire data set and V is the partition based on clustering of a subset of the data set. Let a be the number of pairs of objects that are placed in the same cluster in U and in the same cluster in V, b be the number of pairs of objects that are placed in the same cluster in U but not in the same cluster in V, c be the number of pairs of objects in the same cluster in V but in different clusters in U, and d be the number of pairs of objects in different clusters in both partitions. The Rand index[38] is given by eq 7

$$R_{U,V} = \frac{a + d}{a + b + c + d} \quad (7)$$

A problem with the Rand index is that its expected value for two random partitions does not necessarily take a constant value. As a result, the Rand index can evaluate to unexpectedly high values. This can be overcome by using the adjusted Rand index, as proposed by Hubert and Arabie,[39] which assumes the generalized hypergeometric distribution as a model of
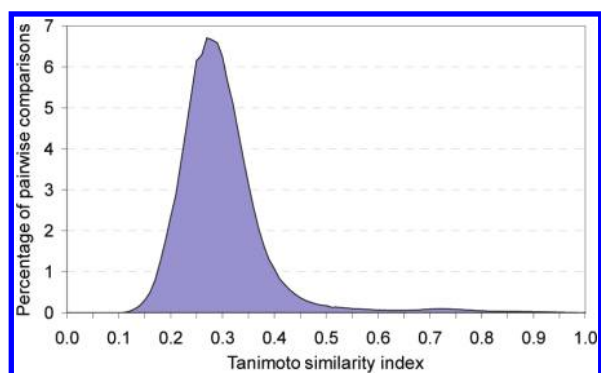
Figure 1. Distribution of Tanimoto similarity values for the complete pairwise comparison of the compound set. Compounds were represented by Daylight fingerprints.

randomness (eq 8)

$$
R_{U,V,adj} = \frac{\sum_{i,j}\binom{n_{ij}}{2} - \left[\sum_i \binom{n_{i.}}{2}\sum_j \binom{n_{.j}}{2}\right]/\binom{n}{2}}{\frac{1}{2}\left[\sum_i \binom{n_{i.}}{2} + \sum_j \binom{n_{.j}}{2}\right] - \left[\sum_i \binom{n_{i.}}{2}\sum_j \binom{n_{.j}}{2}\right]/\binom{n}{2}}
$$

(8)

where n_{ij} is the number of objects of the intersection of class u_i in partition U and class v_j in partition V, $n_{i.}$ is the number of objects in the class u_i in partition U, $n_{.j}$ is the number of objects in the class v_j in partition V, and n is the number of objects in $S = \{O_1,...,O_n\}$.

■ RESULTS AND DISCUSSION

Construction of the Chemogenomics Matrix. The effect of a drug at a certain target does not directly depend on the amino acid sequence of the target but on the local pharmacophoric interaction pattern. There are rare examples of drugs having different, but overlapping binding sites at one target.[41,42] Also, studies of drug side effects suggest that most drugs interact with more than one target.[43] Notably, these targets do not have to be phylogenetically related.

Our chemogenomics panel of GPCR targets was designed to broadly cover the space of pharmaceutically relevant GPCR binding sites, with focus on some particular areas of interest at Boehringer Ingelheim. Following the suggested classification by Surgand and co-workers,[2] we compiled a set of targets representing seven human GPCR clusters of which two clusters contain three targets each, and five clusters are represented by one target: i) the amines cluster (5-hydroxytryptamine 2C receptor, beta-2 adrenergic receptor, muscarinic acetylcholine receptor M3), ii) the adenosine receptor cluster (adenosine A1 receptor), iii) the lipids receptor cluster (cannabinoid receptor 2), iv) the chemokine receptor cluster (C—C chemokine receptor type 3, C-X-C chemokine receptor types 2 and 3), v) the chemoattractants receptor cluster (GPR44), vi) the brain-gut peptides receptor cluster (GPR24), and vii) the opiate receptor cluster (somatostatin receptor type 4) (Table 1).

These eleven targets formed the first axis of our chemogenomics matrix. The second axis was formed by 3519 compounds from the Boehringer Ingelheim screening compound pool. The selection of compounds, for which we already knew that they are active against at least one of our targets, reduces the risk of

Table 2. Number of Multiple Target Hitters with Respect to Different Hit Thresholds

number of targets per compound	number of compounds		
	$IC_{50} < 100\ \mu M$	$IC_{50} < 10\ \mu M$	$IC_{50} < 1\ \mu M$
1	1253	1254	968
2	580	374	76
3	311	211	5
4	211	96	1
5	185	47	0
6	81	7	0
7	23	6	0
8	5	1	0
9	3	0	0
10	1	0	0
11	0	0	0

producing a data set with many completely inactive compounds. To broaden the variety of chemotypes, the compounds were selected as series of diverse scaffolds, rather than picking singletons randomly. This way, we ensure that potential similarities between two targets are not due to a single chemotype and maximize the chance to observe different interaction patterns for each chemotype cluster. For each target up to 110 known actives were retrieved and complemented by additional 210 structurally similar compounds with unknown activities (Figure 1). The distribution of the all-against-all pairwise Tanimoto similarity values peaks at 0.29 (in the interval [0;1]) with a standard deviation of 0.09. This value suggests low average pairwise similarity and structural diversity of the ligand set. A second, notably smaller maximum is found at a Tanimoto value of 0.72 (Figure 1). This smaller peak reflects the local structural compound clusters formed by adding 210 similar compounds to each active ligand class. Only 0.01% of all 164700 pairwise comparisons yielded a Tanimoto value >0.98 (1238 compound pairs).

Experimental Testing. The selected set of 3519 compounds was tested in dose response assays for reference ligand displacement against 11 GPCR targets (Table 1). 2653 compounds were active with an IC_{50} value below 100 μM in at least one assay (Table 2), 1996 compounds yielded an IC_{50} value below 10 μM, and 1050 compounds below 1 μM for at least one target, corresponding to 75%, 57%, and 30% of the compound set, respectively. 1400 compounds exhibited detectable activity in least two assays, 820 hit at least three targets, 509 compounds hit at least four targets, and 298 compounds yielded detectable IC_{50} values for at least five targets. The corresponding numbers for an activity threshold of 10 μM are 742, 368, 157, and 61; and for a threshold of 1 μM the observed compound numbers are 82, 6, 1 and 0, respectively. Even if there are a few compounds with submicromolar affinities, the majority of multitarget hitters exhibit only moderate ($1-10\ \mu M$) or low ($10-100\ \mu M$) affinity.

The scatter plot matrix in Figure 2 presents the distribution of detectable IC_{50} values for all compounds in all assay combinations. Each single scatter plot represents a target pair. The axes are in logarithmic scale with the 1 μM tick mark in the center of each axis. When splitting each scatter plot into four quadrants, the lower left represents compounds with submicromolar IC_{50} values at both targets, and the upper right quadrant represents

1900

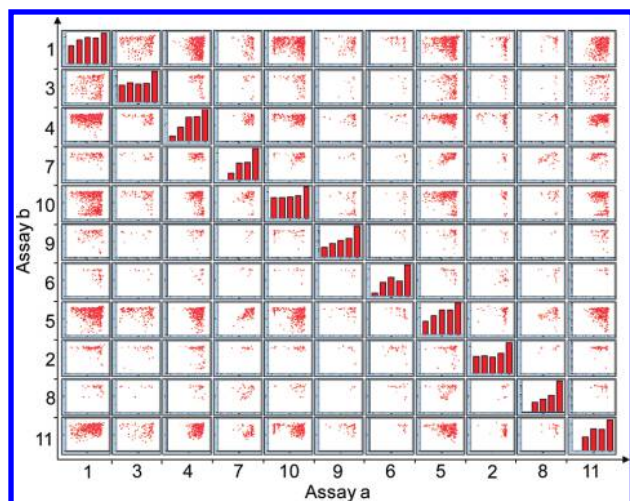dx.doi.org/10.1021/ci200105t |*J. Chem. Inf. Model.* 2011, 51, 1897–1905

Figure 2. Scatter plot matrix of all assay results. The matrix presents the scatter plots of the dose response values of the compound set in assay b (y-axis) versus the dose response values of the compound set in assay a (x-axis). Numbers indicate the targets used for the plots in each row and column, respectively. The corresponding targets, denoted by SwissProt entry name (SwissProt Accession Code in brackets) are as follows: 1: human 5-hydroxytryptamine 2C receptor (5HT2C_HUMAN; P28335), 2: human adenosine A1 receptor (AA1R_HUMAN; P30542), 3: human beta-2 adrenergic receptor (ADRB2_HUMAN; Q9UMZ), 4: human cannabinoid receptor 2 (CNR2_HUMAN; P34972), 5: human C−C chemokine receptor type 3 (CCR3_HUMAN; P51677), 6: human G protein-coupled receptor GPR44 (GPR44_HUMAN; Q9Y5Y4), 7: human C-X-C chemokine receptor type 2 (CXCR2_HUMAN; P25025), 8: human C-X-C chemokine receptor type 3 (CXCR3_HUMAN; P49682), 9: human muscarinic acetylcholine receptor M3 (ACM3_HUMAN; P20309), 10: human G protein-coupled receptor GPR24 (MCHR1_HUMAN; Q99705), 11: human somatostatin receptor type 4 (SSR4_HUMAN; P31391). The axes of each scatterplot give the IC50 values in a logarithmic scale, starting at 0.01 μM and going up to 100 μM, with the point 1 μM in assay a and 1 μM in assay b being exactly in the center of the scatterplot. The main diagonale in the scatterplot matrix presents a histogram of the dose response values of the target of the row/column. The thresholds for each bar in the histograms are from the left to the right: IC50 $\leq$ 0.1 μM, 0.1 μM< IC50 $\leq$ 1 μM, 1 μM< IC50 $\leq$ 10 μM, 10 μM< IC50 < 100 μM, IC50 $\geq$ 100 μM.

compounds with $IC_{50} > 1 \mu$M at both targets. Except for targets 7, 8, and 11, for all other targets potent binders with less or equal 100 nM affinities could be found in the compound set. Targets 1, 2, 3, and 10 show more or less equal distribution of the hits among the selected bins. Apparently, the distribution of IC_{50} values depends on the particular assay pair considered. There are pairs of targets where only hits with low affinities can be observed (e.g., assays 4/11, 8/9, 6/7, 7/9). On the other hand, there are combinations, where the compounds fill the entire scatter plot nearly equally distributed (e.g., 1/3). Some combinations of assays show a spectrum of IC_{50} values where the compounds are equally distributed with respect to one axis but are concentrated in the less active half with respect to the other axis (e.g., 1/4, 1/11, or 2/10). Finally, some plots have hits in all quadrants except for the lower left (compounds with high activity in both assays, e.g. 1/5, 3/10, 4/5). Notably, all combinations of assay pairs exhibit a specific distribution of IC_{50} values.

Analysis of Ligand-Target Similarity. Our approach to quantitatively describe the similarity between two targets or assays can directly be applied to the scatter plot matrix. Apparently two

targets share some similarity if the same compounds are active at both targets. More precisely, two targets are considered as "identical", if the same compounds have the same affinities at both targets. Based on this hypothesis, we developed a quantitative measure, ARTS, that takes multiple aspects of assay related target similarities into account. ARTS (eq 5) is a standardized measure of pairwise target similarity, based on experimental affinities of probe compounds. Each probe compound contributes to the similarity of the respective targets. Based on its affinity data, we calculate a score for each probe compound (eq 4) that on the one hand considers the potency of the experimental data — the score increases with the square of the mean affinity, in which "mean affinity" represents the statistical average of the experimental values for the two respective targets. On the other hand, the score includes the selectivity of the probe compound by applying a Gaussian function that — according to our hypothesis that two targets are similar if the same compounds have the same affinities at both targets — decreases the score for selective compounds. By introducing those two terms into the score, we avoid the use of an arbitrary cutoff value to discriminate between hits and nonhits while at the same time prioritizing more potent compounds. Furthermore we apply a smoothing function that allows even highly selective compounds to contribute to the score with a low weight. This idea is somehow inspired by the signal processing as it is used in the digital image analysis or the audio signal processing. In all those fields Gaussian filters are used for many years. The most common usage of those Gaussian filters is the band-pass filter, which enables frequencies of a certain range to pass the filter and at the same time rejects undesirable frequencies. Our implementation of the Gaussian filter does not completely reject data with unwanted properties, i.e. selectivities, but deprioritizes them. A visualization of the scores for samples of artificial probe compounds can be found in the Supporting Information (Figure S1−S4). The usage of the constant k is motivated but in a way arbitrary and reflects the fact that according to our experience compound concentrations of more than 100 μM can cause unspecific interactions and solubility issues. As a consequence we restrict our assay setup to a cartain maximal concentration. Dose response values that exceed that concentration are primarily reported with an operater and in our preprocessing of the data set to the arbitrary value of 100 μM.

The sum of the scores for all probe compounds represents the raw similarity score for two targets (eq 3). As this score strongly depends on the number of probe compounds for which data exist and on the affinity value distribution, we introduce a standardization factor by dividing the similarity index by the square root of the self-similarity of the respective targets (eq 5). This way we reduce the risk of overestimating those targets for which plenty experimental information is available. Furthermore, we ensure that we scale the assay related similarity index within a reasonable, expectable range. Although the affinity distribution-based score scaling attenuates the strong correlation between the similarity score and the visual impression from the scatter plot, this procedure is necessary to avoid potential misinterpretation due to the lack of active compounds.

The application of the ARTS metric to all combinations of targets gives new and quantitative insights into the relationships of the targets in our chemogenomics panel. Hierarchic clustering of the similarity matrix using Wards clustering procedure is presented in Figure 3a, together with the hierarchical clustering of phylogenetic similarities (Figure 3b). While the resulting
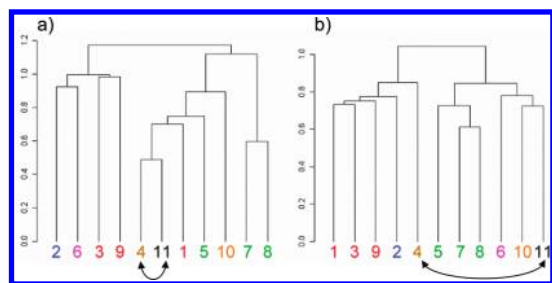
Figure 3. Dendrograms of the targets using Ward-clustering and the ARTS similarity index (a) and Ward-clustering of the phylogenetic similarity of the sequences (b). Numbers correspond to the targets (cf. Table 1). Coloring corresponds to the phylogenetic groups suggested by Surgand et al.[2]: red: amine receptors, blue: adenosine receptors, brown: lipid receptors, green: chemokine receptors, magenta: chemoattractant receptors, orange: brain-gut peptide receptors, black: opiate receptors. Ward's clustering method of the phylogenetic similarity matrix (b) produces clusters that group those targets that are closely related with respect to their amino acid sequence. Targets that have high sequence similarity like the biogenic amine receptors 1, 3, 9 or the chemokine receptors 5, 7, 8 are grouped together. This is not the case for the ARTS similarity metric clustering (a). While the two biogenic amine receptors 3 and 9 show up in the same cluster, the third biogenic amine receptor 1 is found in a different cluster. The chemokine receptor 5 is in a more distant position with respect to the two other chemokine receptors 7 and 8. A major difference between dendrogram a) and dendrogram b) is the position of the lipid receptor cluster target 4 (CB2) and the opiate receptor cluster target 11 (SSTR4). Those GPCRs are located in different clusters in dendrogram b), which is in agreement with their low phylogenetic similarity. In dendrogram a), these targets show the highest degree of similarity.

phylogenetic groups are structurally related (biogenic amine receptors — red, chemokine receptors — green), ARTS based clustering generates different groups of targets. The most obvious difference is the relationship between human cannabinoid receptor 2 (target no. 4 in Figure 3) and somatostatin receptor type 4 (target no. 11 in figure 3). The first one belongs to the lipids receptor cluster, and therefore the placement in relative proximity to the amine receptors and the adenosine receptor in the phylogenetic clustering is completely in line with its phylogenetic relationships. The second one belongs to the opiates receptor cluster and shares some degree of sequence similarity with the brain-gut peptides receptor cluster (24.3% identity with MCH receptor 1) and the chemoattractants receptors (28% identity with GRR44). Therefore, the clustering result presented in Figure 3b, grouping the human somatostatin receptor type 4 with GPR24 (MCH receptor 1) and GPR44, reflects what is known from the sequence relationships of these receptors.[2] Surprisingly, ARTS based hierarchic clustering in Figure 3a identifies targets 4 and 11 as the most similar pair in the entire ensemble. Both targets are grouped together with the human 5-hydroxytryptamine 2C receptor (target 1 in Figure 3), human C—C chemokine receptor type 3 (target 5 in Figure 3), and GPR24 (target 10 in Figure 3). Looking at the scatter plot matrix in Figure 2, targets 4 and 11 indeed exhibit some similarities with respect to the compounds within the data set. On the other hand, target pairs like 1 and 11, 1 and 5, or 1 and 10 seem to share many more compounds, some are even more active than those of the combination of assays 4 and 11. The fact that the ARTS index nevertheless prefers the similarity of the assay pair of assay 11 and assay 4 could be due to the introduced normalization (eq 5).

Assay 1 resulted in a substantial number of hits with an IC_{50} value below 100 nM (leftmost bar of the histogram in the scatter plot matrix presented in Figure 2). Assay 11 did not yield any hits below 100 nM, and assay 4 shows only a few such potent hits. The ARTS index is scaled by the self-similarity of the two assays that form the assay pair. Assays with potent hits have a high value for the self-similarity (eq 6), and therefore the denominator in eq 5 will reach high values. If assays with high self-similarities do not have potent hits in common, the numerator in eq 5 will be low while the denominator gets high values. That way the ARTS index will decrease for those assay pairs where the self-similarity of each assay does not match the similarity of the pair. Therefore the rating prefers the target combination 4 and 11. However, the other assay pairs with noticeable numbers of common hits are also grouped together in the hierarchical clustering in Figure 3a.

Interestingly, the phylogenetically clustered targets like the biogenic amine receptors 1, 3, and 9, and chemokine receptors 5, 7, and 8, that are grouped in Figure 3b, are not arranged in one cluster each in the ARTS based clustering. The two human C-X-C chemokine receptors, type 2 and type 3 (targets 7 and 8 in Figure 3), form a separate cluster in the ARTS based clustering and are separated from the human C—C chemokine receptor type 3 (target 5 in Figure 3). In the phylogenetic based clustering, all three targets are grouped together in one cluster (Figure 3b). A similar observation can be found for the beta-2 adrenergic receptor (target 3 in Figure 3) and the human muscarinic acetylcholine receptor M3 (target 9 in Figure 3). Both biogenic amine receptors are grouped nearby in both clustering schemes, but the third receptor from this cluster, the human 5-hydroxy-tryptamine 2C receptor (target 1 in Figure 3), is separated from the former two in the ARTS based clustering.

Analysis of Data Set Dependency. A crucial point is the question of data set dependency of the clustering result. The relationships, calculated as ARTS indices, are inferred from observed ligand-target interactions. Therefore, the pairwise similarity of the targets depends on the selection of molecular probes. Obviously, elimination of all compounds from the data set that bind to target 4 and target 11 would definitely reduce the calculated similarity of this target pair. However, it needs to be analyzed how strong the intertarget relationship depends on the composition of a probe collection of diverse compounds that show pairwise affinities and cover a broad variety of chemotypes. A way to assess the stability and reproducibility of a similarity descriptor is to carefully look how modified conditions for data set compilation affect the pairwise similarity scores. We compared hierarchical clustering results using dose response values of random samples with the result for the entire compound set using the adjusted Rand index, as suggested by Milligan and Cooper.[40] As comparisons of two partitions depend on the total number of clusters, our comparison was done separately for each cluster level. For each cluster level (except for the first and the last) we calculated the adjusted Rand index. We took the mean adjusted Rand index for all cluster levels as a score for the agreement of the entire clustering of the reduced compound set with the clustering of the entire compound set. This procedure was repeated 100 times with different random selections each time.

For comparison we computed Pearson's correlation and the Tanimoto index. The conservation of global similarities and relationships using these two coefficients as similarity scores for the pairwise comparison of the targets was assessed via the adjusted Rand index, too. The boxplots for the resulting distributions of mean adjusted Rand indices for the ARTS based
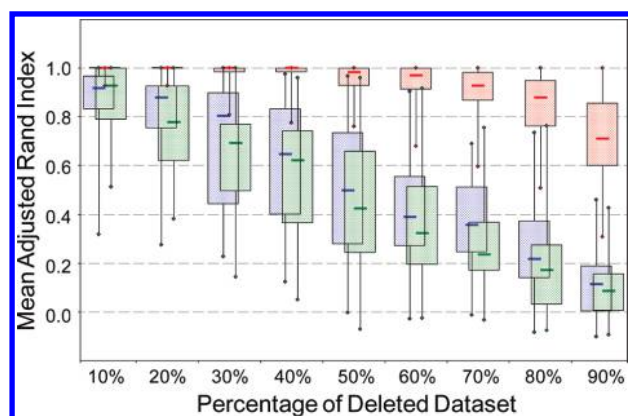
1902

dx.doi.org/10.1021/ci200105t |*J. Chem. Inf. Model.* 2011, 51, 1897–1905

Figure 4. Dependency of the mean adjusted Rand index on the percentage of deleted compounds. The diagram presents boxplots of the distributions of the mean adjusted Rand index of three different indices with different subsets of the data set. Each calculation of the adjusted Rand index was performed with a randomly selected portion of the data set with 100 repetitions. The selection removed all IC_{50} values from the data set for the selected compounds. For each random selection, the calculation of a hierarchical clustering was performed using the ARTS similarity (red), the Tanimoto index (green), and Pearson's correlation coefficient (blue). Each clustering result was compared with the result obtained with the entire data set. Each box plot shows five characteristics of the distribution of the 100 mean adjusted Rand indices for every similarity metric and the particular percentage of the data set that was used. The five characteristics are the first (Q1) and the third quartile (Q3), forming the lower and the upper boundary of the box, respectively, the median or second quartile (Q2), shown as a horizontal bar in the center of the box and the minimum and maximum value, forming the whiskers of the boxplot.

clustering, the Tanimoto coefficient based clustering, and the Pearsons correlation coefficient based clustering for different fractions of the data set are presented in Figure 4. We deleted between 10% and 90% of the data set, in 10% steps. Deletion of 10% of the compounds in the data set had only a marginal effect on the distribution of the adjusted Rand index that was deduced from the ARTS based clustering. Although the minimum mean adjusted Rand index goes down to 0.93, the quartile 1 value (Q1), the median, the quartile 3 value (Q3), and the maximum stay at a value of 1.0. This suggests that at least for 75% of the random selections for the reduced compound set the ARTS based clustering is not different from the clustering of the entire data set. This outcome is the same for the second box plot for the ARTS based clustering, again showing a minimum of 0.93 and a Q1, median, Q3 and a maximum of 1.0. Deleting 30% of the data set reduces the minimum to 0.81, and the Q1 value to 0.98, while the median, Q3 and the maximum stay at 1.0. Deletion of further 10% of the compound set results in a similar distribution with only the minimum value reduced by further 0.03 and Q1 to Q3 and the maximum remaining the same. The use of only 50% of the entire data set still yields clustering results that are very similar to the clustering of the entire data set. At 50% of the data set, the median is slightly decreased by 0.02. The decrease of the value for the median of the mean adjusted Rand index distribution goes on with further reduction of the compound set to 0.97, 0.93, 0.88, and 0.71 for the deletion of 60%, 70%, 80%, and 90% of the data set, respectively. Even with 30% of the compound set, every second random compound collection has a mean adjusted Rand index of 0.93 and higher, indicating a high degree
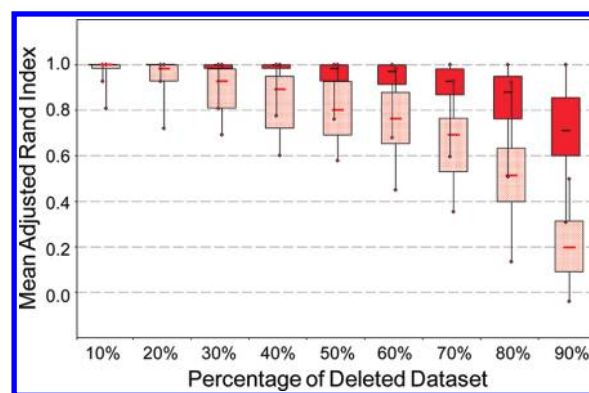

Figure 5. Dependency of the mean adjusted Rand index for the ARTS based clustering on the percentage of deleted compounds or matrix holes. The procedure is the same as described in the legend to Figure 4, deleting 10%, 20% ... up to 90% of the data set and performing a hierarchical clustering on the remaining data. The light red boxplots show the resulting distribution of mean adjusted Rand indices when removing single entries of the matrix of dose response values. The dark red box shows the results for the deletion of entire compounds. Deleting 80% of the compounds results in a similar distribution as deleting of 30% of the data.

of similarity with the clustering result using the entire compound set and ARTS based clustering.

Surprisingly, the grade of consensus of the clustering of the reduced data set and the clustering of the entire data set is remarkably lower with the Tanimoto coefficient or Pearson's correlation coefficient. Even with 90% of the data set (i.e., deletion of only 10%), the median of the distribution of the mean adjusted Rand index for Pearson's correlation coefficient based clustering has a value of 0.93 — comparable with the distribution of the mean adjusted Rand index of the ARTS based clustering at deletion of 70% of the data set. The Tanimoto coefficient is even slightly lower (median = 0.92). Overall, the Tanimoto and Pearson correlation coefficient yield similarity value distributions that decrease faster with increasing reduction of the data set. Although the deviation between Q1 and Q3 increases, Q3 still assumes lower values than Q1 in the ARTS based cluster comparison. These results indicate that the ARTS based clustering might be more stable than the two other similarity scores investigated in this study. Figure 4 shows that the data set can be reduced by a remarkable number of compounds, while the ARTS clustering still yields results that are comparable with the clustering of the entire data set. Although Pearson's correlation coefficient is well accepted as one of the most popular correlation coefficients, it might suffer from some boundary conditions, Pearson defined. Especially the requested normal distribution is a demand that might not be true for dose responsive values. In addition to Pearson's correlation coefficient we performed the analysis for Spearman's rank correlation coefficient (data see the Supporting Information). Surprisingly, the distribution of the mean adjusted Rand index for Spearman's rank correlation coefficient is similar to that for Pearson's correlation coefficient yet even slightly worse.

For a systematic analysis of ARTS relationships between targets the dose response values for all compounds and all targets are required. A more realistic scenario is a less dense matrix containing missing data. How well does ARTS clustering perform with such a setting? Figure 5 presents the direct comparison
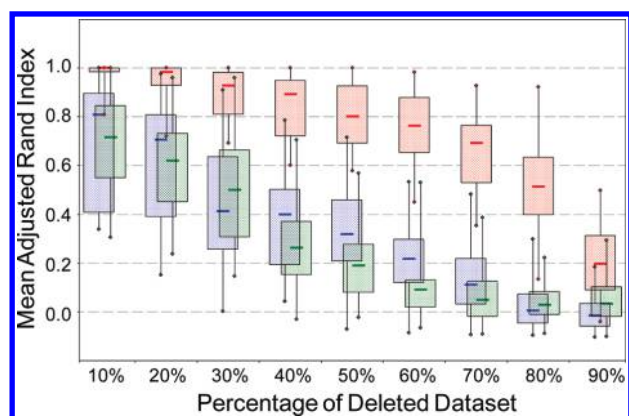
Figure 6. Dependency of the mean adjusted Rand index on the percentage of deleted data for three different similarity indices: ARTS (red), Tanimoto (green), Pearsons correlation (blue).

of ARTS clustering with the data set being reduced compound-wise (filled box plots) and with the ARTS clustering of a sparse matrix. The latter was generated by randomly deleting dose response values. Apparently, less dense matrices result in less reproducible clusterings, as indicated by the more rapid decrease of the median of the distributions of the clustering results for matrices with higher percentage of deleted data points and the broader variability of the mean adjusted Rand indices. The distribution of mean adjusted Rand indices of a matrix with 20% missing values is comparable with the distribution that results after deletion of 50% of the compounds. Q1 (0.93), Q2 (0.98), and Q3 (1.0) are identical in both distributions, and the minimum of the distribution with a holey matrix is slightly lower (0.72) than the comparable value for the compound-reduced matrix (0.76). Again the Tanimoto index and Pearson correlation coefficient as similarity measures seem to be less suited for this experimental setting (Figure 6).

CONCLUSIONS

Known ligands of similar targets might be useful starting points for the identification of novel ligands for a target of interest. The knowledge of target similarities can also be helpful in analyzing ligand side effects and might lead to the repurposing of known drugs. For these and other applications of chemogenomics knowledge, the target similarity must be defined on a meaningful basis. ARTS represents a similarity index for sequence-independent similarity estimation. We could demonstrate that the ARTS relationship of eleven pharmaceutically relevant GPCRs correlates better with the results of SPA assays than sequence based target similarity. We also showed that the ARTS relationships of the selected targets are relatively stable with respect to the composition of the probe compounds. With a reduced compound set containing only 40% of the entire ensemble it was still possible to obtain reproducible target similarities. This sparsity level corresponds to roughly 130 diverse compounds per target. ARTS based intertarget similarities appear to be less susceptible to incomplete data sets than Pearson correlation or the Tanimoto index. It will be useful to investigate whether a similar scoring scheme on the basis of less accurate data than dose response values is meaningful. This possibility could dramatically decrease the effort and expenses of the chemogenomics approach. We wish to stress that ARTS represents a scheme to compare assay results. Only in cases where the assay readout is

mainly affected by the ligand binding process, as e.g. in displacement assays, ARTS results give a hint to the similarity of targets.

ASSOCIATED CONTENT

S **Supporting Information.** List of all dose responsive values. The chemogenomics matrix is presented as a table of pIC_{50} values for each compound with the anonymized compound code in the first column and the dose responsive values in the further columns. The respective target is mentioned in the respective column header. Samples whose dose responsive value exeeds the assay conditions are reported as '$pIC_{50} = 4$'. An exemplary set of four distributions of artificial assay pairs to better understand the behavior of the equation for the score in the ARTS equation is shown in Figure S1−S4. The data from Figure 4 are listed in Table S1a-S1b. In addition to the three similarity coefficients from Figure 4, Table S1b contains the data for Spearman's rank correlation coefficient. This material is available free of charge via the Internet at http://pubs.acs.org.

AUTHOR INFORMATION

Corresponding Author
*E-mail: michael.bieler@boehringer-ingelheim.com.

ACKNOWLEDGMENT

REFERENCES

(1) Gloriam, D. E.; Foord, S. M.; Blaney, F. E.; Garland, S. L. Definition of the G protein-coupled receptor transmembrane bundle binding pocket and calculation of receptor similarities for drug design. *J. Med. Chem.* **2009**, *52*, 4429–4442.

(2) Surgand, J. S.; Rodrigo, J.; Kellenberger, E.; Rognan, D. A chemogenomic analysis of the transmembrane binding cavity of human G-protein-coupled receptors. *Proteins* **2006**, *62*, 509–538.

(3) Bajorath, J. Computational analysis of ligand relationships within target families. *Curr. Opin. Chem. Biol.* **2008**, *12*, 352–358.

(4) Bender, A.; Jenkins, J. L.; Glick, M.; Deng, Z.; Nettles, J. H.; Davies, J. W. "Bayes affinity fingerprints" improve retrieval rates in virtual screening and define orthogonal bioactivity space: when are multitarget drugs a feasible concept? *J. Chem. Inf. Model.* **2006**, *46*, 2445–2456.

(5) Schneider, G.; Tanrikulu, Y.; Schneider, P. Self-organizing molecular fingerprints: a ligand-based view on drug-like chemical space and off-target prediction. *Future Med. Chem.* **2009**, *1*, 213–218.

(6) Bender, A.; Young, D. W.; Jenkins, J. L.; Serrano, M.; Mikhailov, D.; Clemons, P. A.; Davies, J. W. Chemogenomic data analysis: prediction of small-molecule targets and the advent of biological fingerprint. *Comb. Chem. High Throughput Screening* **2007**, *10*, 719–731.

(7) Gregori-Puigjane, E.; Mestres, J. A ligand-based approach to mining the chemogenomic space of drugs. *Comb. Chem. High Throughput Screening* **2008**, *11*, 669–676.

(8) Jacob, L.; Vert, J. P. Protein-ligand interaction prediction: an improved chemogenomics approach. *Bioinformatics* **2008**, *24*, 2149–2156.

(9) Pirard, B. Structure-based chemogenomics: analysis of protein family landscapes. *Methods Mol. Biol.* **2009**, *575*, 281–296.

(10) Strombergsson, H.; Kleywegt, G. J. A chemogenomics view on protein-ligand spaces. *BMC Bioinf.* **2009**, *10* (Suppl 6), S13.

(11) Caron, P. R.; Mullican, M. D.; Mashal, R. D.; Wilson, K. P.; Su, M. S.; Murcko, M. A. Chemogenomic approaches to drug discovery. *Curr. Opin. Chem. Biol.* **2001**, *5*, 464–470.

(12) Schuffenhauer, A.; Jacoby, E. Annotating and mining the ligand-target chemogenomics knowledge space. *Drug Discovery Today: BIOSILICO* **2004**, *2*, 190–200.

(13) Rognan, D. Chemogenomic approaches to rational drug design. *Br. J. Pharmacol.* **2007**, *152*, 38–52.

(14) Receveur, J. M.; Bjurling, E.; Ulven, T.; Little, P. B.; Norregaard, P. K.; Hogberg, T. 4-Acylamino-and 4-ureidobenzamides as melanin-concentrating hormone (MCH) receptor 1 antagonists. *Bioorg. Med. Chem. Lett.* **2004**, *14*, 5075–5080.

(15) Caron, P. R.; Mullican, M. D.; Marshal, R. D.; Wilson, K. P.; Su, M. S.; Murcko, M. A. Chemogenomics, a gene family approach to parallel drug discovery. *Drug Discovery World Fall* **2001**, 57–62.

(16) Klabunde, T. Chemogenomic approaches to drug discovery: similar receptors bind similar ligands. *Br. J. Pharmacol.* **2007**, *152*, 5–7.

(17) Azzaoui, K.; Hamon, J.; Faller, B.; Whitebread, S.; Jacoby, E.; Bender, A.; Jenkins, J. L.; Urban, L. Modeling promiscuity based on in vitro safety pharmacology profiling data. *ChemMedChem* **2007**, *2*, 874–880.

(18) Bender, A.; Scheiber, J.; Glick, M.; Davies, J. W.; Azzaoui, K.; Hamon, J.; Urban, L.; Whitebread, S.; Jenkins, J. L. Analysis of pharmacology data and the prediction of adverse drug reactions and off-target effects from chemical structure. *ChemMedChem* **2007**, *2*, 861–873.

(19) Crossley, R. The design of screening libraries targeted at G-protein coupled receptors. *Curr. Top. Med. Chem.* **2004**, *4*, 581–588.

(20) Crossley, R.; Rose, V.; Stevens, A. P. Compound libraries. WO-03004147, 2003.

(21) Kauvar, L. M.; Higgins, D. L.; Villar, H. O.; Sportsman, J. R.; Engqvist-Goldstein, A.; Bukar, R.; Bauer, K. E.; Dilley, H.; Rocke, D. M. Predicting ligand binding to proteins by affinity fingerprinting. *Chem. Biol.* **1995**, *2*, 107–118.

(22) Briem, H.; Kuntz, I. D. Molecular similarity based on DOCK-generated fingerprints. *J. Med. Chem.* **1996**, *39*, 3401–3408.

(23) Guba, W.; Green, L. G.; Martin, R. E.; Roche, O.; Kratochwil, N.; Mauser, H.; Bissantz, C.; Christ, A.; Stahl, M. From astemizole to a novel hit series of small-molecule somatostatin 5 receptor antagonists via GPCR affinity profiling. *J. Med. Chem.* **2007**, *50*, 6295–6298.

(24) Martin, R. E.; Green, L. G.; Guba, W.; Kratochwil, N.; Christ, A. Discovery of the first nonpeptidic, small-molecule, highly selective somatostatin receptor subtype 5 antagonists: a chemogenomics approach. *J. Med. Chem.* **2007**, *50*, 6291–6294.

(25) Poroikov, V. V.; Filimonov, D. A.; Borodina, Y. V.; Lagunin, A. A.; Kos, A. Robustness of biological activity spectra predicting by computer program PASS for noncongeneric sets of chemical compounds. *J. Chem. Inf. Comput. Sci.* **2000**, *40*, 1349–1355.

(26) Martynova, N. B.; Filimonov, D. A.; Poroikov, V. V. Computer prediction of biological activity spectra for low-molecular peptides and peptidomimetics. *Bioorg. Khim.* **2000**, *26*, 330–339.

(27) Bock, J. R.; Gough, D. A. Virtual screen for ligands of orphan G protein-coupled receptors. *J. Chem. Inf. Model.* **2005**, *45*, 1402–1414.

(28) Mestres, J.; Martin-Couce, L.; Gregori-Puigjane, E.; Cases, M.; Boyer, S. Ligand-based approach to in silico pharmacology: nuclear receptor profiling. *J. Chem. Inf. Model.* **2006**, *46*, 2725–2736.

(29) Schneider, G.; Tanrikulu, Y.; Schneider, P. Self-organizing molecular fingerprints: a ligand-based view on drug-like chemical space and off-target prediction. *Future Med. Chem.* **2009**, *1*, 213–218.

(30) Tanrikulu, Y.; Kondru., R.; Schneider, G.; So, W. V.; Bitter, H. M. Missing value estimation for compound-target activity data. *Mol. Inf.* **2010**, *29*, 678–684.

(31) Daylight. http://www.daylight.com/ (accessed June 1, 2011).

(32) Alouani, S. Scintillation proximity binding assay. *Methods Mol. Biol.* **2000**, *138*, 135–141.

(33) Jessop, R. A. Imaging proximity assays. *Proc. SPIE-Int. Soc. Opt. Eng.* (Systems and Technologies for Clinical Diagnostics and Drug Discovery) **1998**, *3259*, 228-233.

(34) Sorg, G.; Schubert, H. D.; Buttner, F. H.; Heilker, R. Automated high throughput screening for serine kinase inhibitors using a LEADSeeker scintillation proximity assay in the 1536-well format. *J. Biomol. Screening* **2002**, *7*, 11–19.

(35) Ramm, P. Imaging systems in assay screening. *Drug Discovery Today* **1999**, *4*, 401–410.

(36) *Pipeline Pilot*, version 7.5.2; Accelrys: San Diego, CA, 2008.

(37) R. http://www.r-project.org/ (accessed June 1, 2011).

(38) Rand, W. M. Objective Criteria for the Evaluation of Clustering Methods. *J. Am. Stat. Assoc.* **2009**, *66*, 846–850.

(39) Hubert, L.; Arabie, P. Comparing Partitions. *J. Classif.* **1985**, *2*, 193–218.

(40) Milligan, G. W.; Cooper, M. C. A study of the comparability of external criteria for hierarchical cluster analysis. *Multivar. Behav. Res.* **1986**, *21*, 441–458.

(41) Betz, S. F.; Reinhart, G. J.; Lio, F. M.; Chen, C.; Struthers, R. S. Overlapping, nonidentical binding sites of different classes of nonpeptide antagonists for the human gonadotropin-releasing hormone receptor. *J. Med. Chem.* **2006**, *49*, 637–647.

(42) Greenfeder, S.; Cheewatrakoolpong, B.; Anthes, J.; Billah, M.; Egan, R. W.; Brown, J. E.; Murgolo, N. J. Two related neurokinin-1 receptor antagonists have overlapping but different binding sites. *Bioorg. Med. Chem.* **1998**, *6*, 189–194.

(43) Hert, J.; Keiser, M. J.; Irwin, J. J.; Oprea, T. I.; Shoichet, B. K. Quantifying the relationships among drug classes. *J. Chem. Inf. Model.* **2008**, *48*, 755–765.